Schulz, H.-M., Wirth, R., Schreiber, A. (2016): Organic-inorganic rock-fluid interactions in stylolitic micro-environments of carbonate rocks: A FIB-TEM study combined with a hydrogeochemical modelling approach. - *Geofluids*, *16*, 5, pp. 909–924.

DOI: http://doi.org/10.1111/gfl.12195

GEOFLUIDS

Geofluids (2016) **16**, 909–924 doi: 10.1111/gfl.12195

Organic–inorganic rock–fluid interactions in stylolitic micro-environments of carbonate rocks: a FIB-TEM study combined with a hydrogeochemical modelling approach

H.-M. SCHULZ[1], R. WIRTH[2] AND A. SCHREIBER[3]

[1]*Sec. 3.2 Organic Geochemistry, Helmholtz Centre Potsdam – GFZ German Research Centre for Geosciences, Potsdam, Germany;* [2]*Sec. 4.3 Chemistry and Physics of Earth Materials, Helmholtz Centre Potsdam – GFZ German Research Centre for Geosciences, Potsdam, Germany;* [3]*Sec. 4.2 Geomechanics and Rheology, Helmholtz Centre Potsdam – GFZ German Research Centre for Geosciences, Potsdam, Germany*

ABSTRACT

Stylolites and the interfaces to the host limestone have been investigated by means of a multidisciplinary analytical approach (thin section microscopy, FIB-TEM, organic geochemistry and petrography). Carbonate dissolution assuming different boundary conditions was simulated by applying a generic hydrogeochemical modelling approach. It is the conceptual approach to characterize and quantify traceable organic–inorganic interactions in stylolites dependent on organic matter type and its thermal maturity, and to follow stylolite formation in carbonates as result of organic matter reactivity rather than pressure solution as a main control. The investigated stylolite samples are of Upper Permian (Lopingian, Zechstein), Middle Triassic (Muschelkalk) and Late Cretaceous (Maastrichtian) age and always contain marine organic matter. The thermal maturity of the organic matter ranges from the pre-oil generation zone (0.4–0.5% R_r) to the stage of dry gas generation (>1.3% R_r). The results of the generic hydrogeochemical modelling indicate a sharp increase of calcite dissolution and the beginning of stylolite formation at approximately 40°C, which is equivalent to a depth of less than 800 m under hydrostatic conditions considering a geothermal gradient of 30°C and a surface mean temperature of 20°C. This temperature corresponds to the pre-oil window when kerogens release an aqueous fluid enriched in carbon dioxide and organic acids. This aqueous fluid may change the existing pore water pH or alkalinity and causes dissolution of carbonate, feldspar and quartz, and clay mineral precipitation along the stylolite. Dissolution of limestone and dolostone leads to reprecipitation of calcite or dolomite opposite of the dissolution side, which indicates only localized mass redistribution. All these integrated hydrogeochemical processes are coupled to the generation of water during organic matter maturation. In all of the calculated hydrogeochemical scenarios, H_2O is a reaction product and its formation supports the suggested hypothesis.

Key words: acetic acid, carbon dioxide, carbonate, dissolution, maturation, organic carbon, stylolite, water

Received 27 April 2016; accepted 17 August 2016

Corresponding author: Hans-Martin Schulz, Sec. 3.2 Organic Geochemistry, Helmholtz Centre Potsdam – GFZ German Research Centre for Geosciences, Telegrafenberg, Potsdam D-14473, Germany.
Email: schulzhm@gfz-potsdam.de. Tel: +49 331 288 1789. Fax: +49 331 288 1782.

Geofluids (2016) **16**, 909–924

INTRODUCTION

Stylolites occur frequently in carbonates, in siliciclastic rocks (e.g. Thomas *et al.* 1993; Nenna & Aydin 2011) or in evaporites (e.g. Peryt *et al.* 1993; Bäuerle *et al.* 2000). Traditional hypotheses to explain stylolite formation in carbonates are based on the concept that overburden pressure is the main control as these serrated surfaces often occur parallel to bedding (Railsback 1993; Moore & Wade 2013).

Organic matter is often found at such interfaces (e.g. Von Bergen & Carozzi 1990; Gao *et al.* 1999; Alsharhan & Sadd 2000), but its maturation products were rarely investigated and reported as the driving force of stylolite formation (e.g. Dunham & Larter 1981; and further references in chapter 2). It is thus the aim of this manuscript to investigate stylolite formation in carbonates as a result of organic matter reactivity rather than pressure solution. To reach this goal we applied the conceptual

approach to characterize and quantify traceable organic-inorganic interactions in stylolites dependent on organic matter type and thermal maturity.

Organic–inorganic rock–fluid interactions are described for a variety of geochemical processes in sedimentary basins such as biogenic methane formation (Arning *et al.* 2011), oil degradation (Seewald 2003) or H_2S formation (Fu *et al.* 2016). In such scenarios, soluble hydrocarbons and their alteration products change the hydrogeochemical properties of the formation water, thereby launching multiple inorganic reactions causing the dissolution or the precipitation of minerals (Surdam *et al.* 1989; Prochnow *et al.* 2006). These aqueous fluids form during early diagenesis and early kerogen maturation, and are enriched in carbon dioxide (CO_2), methane (CH_4) and low molecular weight organic acids (LMWOAs; Cooles *et al.* 1987; di Primio & Skeie 2004; Mazzullo & Harris 2009). Such processes can also take place at the interface between organic matter-bearing clayey layers and a carbonate matrix, which is the actual situation before stylolite formation. In any case, water is essential for the process of stylolite formation as it serves as the reactor for geochemical processes. At depths >1000 m and due to cracking reactions before, during and after the main stage of hydrocarbon generation, type II and III kerogens release significant H_2O amounts (also found in artificial maturation experiments, e.g. Lorant & Behar 2002; Vandenbroucke & Largeau 2007). Accordingly, dissolved organic compounds may create chemical micro-environments which allow dissolution and diffusion of dissolved ions, but also precipitation.

Here, we report about investigations of organic–inorganic interactions and their potential role for the formation of stylolites in carbonate rocks. It is the aim of this contribution to unravel such interactions in micro-environments of carbonate rocks and to answer the following questions:

(1) What are the characteristics of organic matter in stylolites, and is there evidence that organic matter maturation products (OMP) control stylolite formation?
(2) Is it possible to track organic–inorganic rock–fluid interactions in stylolites and the adjacent carbonate matrix?
(3) Do maturation products of organic matter (in other words: are pre-oil and early oil released CO_2, CH_4 and LMWOAs) control stylolite generation?
(4) Is the dissolved carbonate precipitated as cement in close vicinity rather than being transported over long distances?
(5) Is it possible to calculate stylolite formation in the form of calcite dissolution rates by hydrogeochemical modelling of organic–inorganic rock–fluid interactions based on chemical thermodynamics? Do such results allow a depth or temperature estimation when calcite starts to dissolve?

ORGANIC–INORGANIC ROCK–FLUID INTERACTIONS DURING STYLOLITE FORMATION – A BRIEF REVIEW

First considerations of organic matter as a main control showed that total organic carbon (TOC)-rich mudstones have a greater sensitivity for stylolite formation than TOC-poorer grainstones (Dunham & Larter 1981). The interpretation of the results led to the hypothesis that carbon dioxide and low molecular organic acids released during organic matter maturation may have led to carbonate dissolution and stylolite formation (for organic acid generation cf. Barth *et al.* 1988). Furthermore, Dunham & Larter (1981) suggested that the subsurface temperature may be more important than the prevailing pressure regime. Such a concept would contradict predictions of stylolite formation to minimum depths of around 700–800 m (Lind 1993; Nicolaides & Wallace 1997).

The aforementioned results from previous studies suggest that there are two major interacting factors for stylolite formation in carbonates: (i) pore water and (ii) organic matter and its diagenetic products. Similar factors also occur at oil–water contacts (OWC) in carbonate oil reservoirs. For example, the occurrence of stylolites in Lower Cretaceous carbonate oil reservoirs in UAE is focussed on the flanks of anticlines rather than on the crest, and the amplitude of these rough dissolution surfaces is highest in the water leg, lower in the oil leg and small in the gas leg (Alsharhan & Sadd 2000; Paganoni *et al.* 2016), but may be due to downward migration of acidic and corrosive fluids (ACF) generated by oil degradation at OWC.

Moore & Wade (2013) and Mazzullo & Harris (2009) hypothesized that CO_2 and organic acids which are generated via decarboxylation of organic matter in source rocks may cause dissolution before the main stage of hydrocarbon filling and that the dissolved carbonate is reprecipitated as a cement in proximity to the site of dissolution. For instance, acetic acid concentrations influence the pH of formation water which controls CO_2 partial pressure (pCO_2) and thus calcite dissolution or precipitation (Lundegard & Land 1989; van Berk *et al.* 2015). However, this process is dependent on temperature. The higher the temperature, the less is the content of acetic acid to cause calcite dissolution (Lundegard & Land 1989).

Petroleum generation and expulsion from stylolites was investigated in a series of papers by di Primio & Leythaeuser (1995), Hofmann & Leythaeuser (1995), and Leythaeuser *et al.* (1995). The results were interpreted based on the consideration that basically homogenous source rocks undergo effective carbonate redistribution due to pressure solution. This concept would require substantial mass transfer due to large volumes and flow rates of formation water to shift solutes.

Clay minerals are regarded as catalysts of carbonate pressure solution, and clay-enriched layers often contain organic matter (e.g. Leythaeuser *et al.* 1995). The relationship between stylolite occurrence and organic matter points to a control of carbonate dissolution by organic diagenetic products, for example, by CO_2 or acetic acid (Lundegard & Land 1989; Metcalf *et al.* 2005; Smith *et al.* 2013). However, if such processes play a significant role, then the presence of water as the reactor for hydrogeochemical processes is crucial.

CONCEPTUAL APPROACH

Sample selection

Stylolite-bearing carbonates (calcitic or dolomitic as host rock) of different stratigraphic levels and depth have been selected to investigate the role of diagenetic organic matter maturation on stylolite formation. Oriented samples were taken from outcrops in actively mined quarries or from borehole cores, and are of well-defined stratigraphic levels. Samples have been taken from Lopingian (Upper Permian Ca1 and Ca2), Late Cretaceous and Middle Triassic strata. The present-day depths of the samples range from surface to 3344 m, but do not represent maximum burial depth in all cases (Table 1).

Analytical techniques

Samples were sawed perpendicular to bedding to prepare polished thin sections which were used to prepare electron transparent TEM foils using the focused ion beam (FIB) technique (Wirth 2004, 2009). The investigated FIB cut TEM foils have the dimensions $15 \times 10 \times 0.150$ μm.

TEM was performed in a Tecnai F20 X-Twin transmission electron microscope with an acceleration voltage of 200 kV. A Schottky field emitter was used as an electron source. The TEM is equipped with a Gatan Tridiem energy filter, a Fishione high-angle annular dark-field detector (HAADF) and an EDAX X-ray analyser with ultrathin window. Minerals were identified by chemical composition (EDS spectra) and from electron diffraction data. High-resolution lattice fringe images in low-indexed zone axis orientation were processed by applying a fast Fourier transform (FFT) to calculate diffraction pattern.

Table 1 Origin of the investigation material.

Sample no.	GFZ sample no.	TEM sample no.	Name	Stratigraphy	Location	Basin or tectonic structure	Sample origin	Today's depth (m)
Chalk-1a	G015404	4361	Hidra Formation	Cenomanian	Danish North Sea	Mona Ridge	Well Mona-1	3344.00 m
Chalk-1b	G015405	4352	Hidra Formation	Cenomanian	Danish North Sea	Mona Ridge	Well Mona-1	3344.00 m
Schaumkalk-1a	G015500	2082	Muschelkalk	Middle Triassic	Rüdersdorf, Brandenburg, Germany	East German Basin	Active quarry	Surface*
Schaumkalk-1b	G015502	4284	Muschelkalk	Middle Triassic	Rüdersdorf, Brandenburg, Germany	East German Basin	Active quarry	Surface*
Ca2-1a	G015406	4082	Ca2 dolomite	Upper Permian	Ührde, Lower Saxony, Germany	Lower Saxony Basin	Active quarry	Surface†
Ca2-1b	G015407	4089	Ca2 dolomite	Upper Permian	Ührde, Lower Saxony, Germany	Lower Saxony Basin	Active quarry	Surface†
Ca2-1c	G015408	4178	Ca2 dolomite	Upper Permian	Ührde, Lower Saxony, Germany	Lower Saxony Basin	Active quarry	Surface†
Ca2-1d	G015409	4176	Ca2 dolomite	Upper Permian	Ührde, Lower Saxony, Germany	Lower Saxony Basin	Active quarry	Surface†
Ca2-2	G015410	4321	Ca2 dolomite	Upper Permian	Mecklenburg Vorpommerania, Germany	East German Basin	Well Pa 1/68	4640.2 m
Ca2-3	G015412	4319	Ca2 dolomite	Upper Permian	Mecklenburg Vorpommerania, Germany	East German Basin	Well Ba 1/63	2822.8 m
Ca1-1a	G015416	4253	Ca1 carbonate	Upper Permian	Luckenwalde, Brandenburg, Germany	East German Basin	Well E Lw 1/80	1821.0 m‡
Ca1-1b	G015417	4244	Ca1 carbonate	Upper Permian	Luckenwalde, Brandenburg, Germany	East German Basin	Well E Lw 1/80	1821.0 m‡
Ca1-2a	G015418	4257	Ca1 carbonate	Upper Permian	Luckenwalde, Brandenburg, Germany	East German Basin	Well E Lw 1/80	1821.0 m‡
Ca1-2b	G015419	4255	Ca1 carbonate	Upper Permian	Luckenwalde, Brandenburg, Germany	East German Basin	Well E Lw 1/80	1821.0 m‡

*Above a salt diapir, about 2000 m uplifted (Schretzenmayr *et al.* 1987). †More than 600–800 m uplifted (R. Müller, 2015, personal communication). ‡More than 1000 m uplifted during Upper Cretaceous, later only slightly ongoing burial (Schretzenmayr *et al.* 1987).

In order to investigate the visible content, type and distribution of organic matter in the stylolites and surrounding sediments, all samples were cut perpendicular to the bedding plane, embedded in epoxy resin and polished. Samples were analysed under reflected white light and UV light illumination using a Zeiss Axioplan microscope equipped with a XBO 75 W/HBO 100 W lamp emitting 546 nm monochromatic light. Microscopy was performed using oil immersion objectives with Zeiss Immersol N immersion oil. Photographs were acquired with an AxioCam camera attached to the microscope and documented using the AxioVision software.

For selected samples, TOC content measurements (Leco SC-632 instrument) and Rock-Eval pyrolysis parameters S1, S2, S3 and T_{max} (Rock-Eval 6 instrument) were determined at Applied Petroleum Technology AS, Norway.

Hydrogeochemical modelling

The generic model approach shall calculate at which temperature (and pressure) calcite dissolution significantly starts, and how much OMP are needed. The modelling approach is adapted to the conceptual approach by van Berk *et al.* (2015). Here, a modified and simplified approach of a 1D reactive transport model across a TOC-rich shale/calcite carbonate interface is calculated for different TOC contents (in the input file represented as 0.1, 1 and 10 moles of OMP), and different pressure and temperature conditions (from 30°C/75 bar to 80°C/300 bar).

Conceptually, OMP (CH_4, CO_2, H_2 and acetic acid) are generated in an organic matter-bearing clayey layer and are released into the adjacent carbonate layer (here pure calcite) by advection. According to van Berk *et al.* (2015), the initial relative kerogen maturation products (KMP) ratios are 1.9 for CO_2, 0.9 for CH_4, 5.0 for H_2 and 0.1 for acetic acid.

During modelling step 1 (see appendix for steps 1, 2 and 3 of the exemplary scenario considering the input of 1.0 mol KMP at 50°C and 150 bar), these KMP dissolve in 1 l of a 1 molal NaCl aqueous solution in a first step in a '0D' batch model reactor under the predefined temperature and pressure conditions. This reactor simulates the conditions in an organic matter-bearing clayey layer. The reactions take place between the mineral phases (0.48 mol each of quartz and kaolinite; 0.01 mol each of calcite, anorthite, albite and K-feldspar) and a potentially coexisting multicomponent gas ($CH_{4(g)}$, $CO_{2(g)}$ and $H_{2(g)}$). In a next, 0.1, 1 or 10 KMP, moles are added to the aqueous solution. Based on the chemical thermodynamics of aqueous equilibrium reactions, the equilibrium species distribution and the mass conversion resulting from these interactions are calculated.

The calcite saturation for the different temperature and pressure conditions is calculated during modelling step 2. In modelling step 3, the calcite carbonate is generically represented by one cell with a pore volume of 1.0 l and a porosity of 10%. According to van Berk *et al.* (2015), advection is simulated by the number of displaced pore volumes (here: $n = 1000$) and simulates the number of events during which the inflowing ACF completely displace the solution which filled the pore volume of the cells before. After each inflow event, the chemical re-equilibration among the new aqueous solution in the pores, the mineral matrix and the gas alters the composition of the system. Steady state flow conditions are one integral prerequisite for this kind of one-dimensional reactive mass transport modelling. Furthermore, mass fluxes and constant initial composition of the ACF influx into the generic carbonate matrix are taken into account.

The batch and the one-dimensional reactive mass transport models were calculated by applying the USGS Phreeqc Interactive 3.1.4-8929 computer code (Parkhurst & Appelo 2013) under implementation of the phreeqc.dat database. As the code is based on the chemical thermodynamics of aqueous equilibrium reactions, it was used to calculate the equilibrium species distribution dependent on different pressure and temperature conditions, and to calculate mass conversion and coupled 1D-advective mass transport.

van Berk *et al.* (2015) pointed out that all acetate-bearing species and a few aqueous aluminium- and silicon-bearing species are not included in the phreeqc.dat database and that they are taken from the minteq.v4.dat database of Phreeqc Interactive 3.1.4-8929 and additionally defined in the input files.

RESULTS

Organic petrography and geochemistry

All investigated stylolites contain – partly few – particulate hydrogen-rich, predominantly aliphatic, oil-prone liptinitic organic material of different thermal maturity which can be visualized by UV illumination and well distinguished from the fluorescence of the host carbonate. A thermal maturity of approximately 0.5% R_r is obvious from the bright green to yellow fluorescence of liptinite in the stylolite of the Late Cretaceous Chalk from the Danish North Sea (Fig. 1B). The samples are from a depth of 3344 m (well Mona-1; Table 1), and the vitrinite reflectance of ca. 0.5% R_r fits the measured data in this well (Petersen *et al.* 2010). A slightly higher thermal maturity of around 0.6% R_r can be tracked for the Schaumkalk samples (Middle Triassic; Fig. 1C). Their hydrogen index (HI) values of around 90 mg HC/g TOC and low oxygen index (OI) values of around 60 mg CO_2/g TOC could suggest questionable terrestrial organic matter which is slightly thermally mature (early oil window maturity; T_{max}: 436°C).

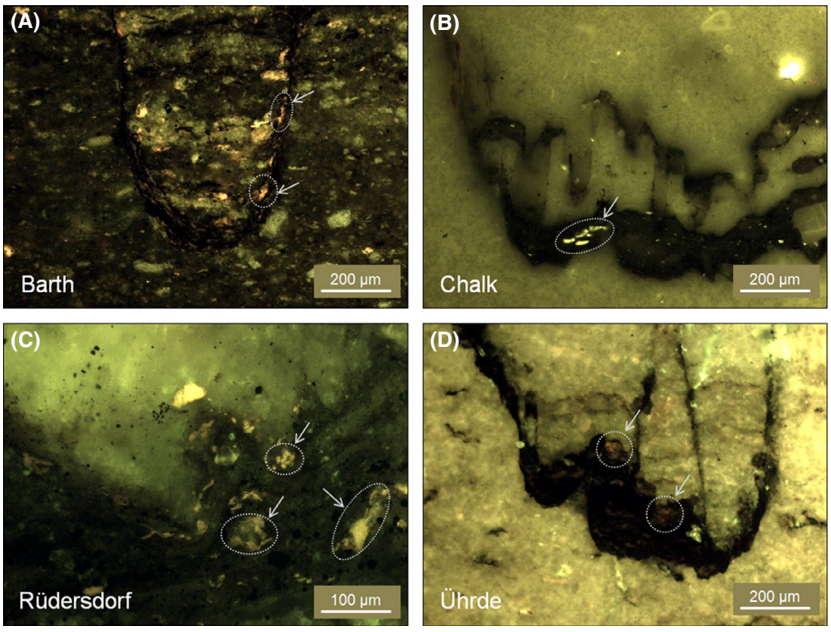

Fig. 1. UV illumination of selected samples showing the occurrence of fluorescing organic matter in the clayey stylolite interface. (A) Sample Ca2-3. (B) Sample Chalk-1. (C) Sample Schaumkalk-1a. (D) Sample Ca2-1.

However, the stylolite samples isolated from Schaumkalk are low in TOC content (0.2 wt.%), and any interpretation of the corresponding Rock-Eval in terms of kerogen type has to be critically evaluated. Significant higher thermal maturities can be followed by lower intense and orange fluorescence such as in the Ca2 dolomite (Upper Permian) in borehole Ba 1/63 (Fig. 1A), which points to peak oil window with around 1.0% R_r (Table 2).

A limiting factor in applying Rock-Eval pyrolysis to determine T_{max} values, which in combination with HI values allow the determination of the organic matter type and thermal maturity, is the partly few stylolitic clayey materials. Accordingly, a mineral matrix effect can falsify the Rock-Eval data which might be the case as for the Ca2 dolomite (Upper Permian) samples from Ührde quarry. The Rock-Eval analysis of this stylolitic material resulted in a T_{max} value of 420°C (Table 2) which indicates immature thermal maturities. However, the fluorescence intensity and colour (Fig. 3D) resemble that in Barth case (Fig. 1A).

Microstructural features

The investigated stylolites show different upper and lower contacts to the host carbonate rocks. Tight carbonate areas may occur above or below the stylolites (Fig. 2B,C). The

Table 2 Carbonate lithology, organic matter, thermal maturity and maximum burial depth of the investigation material.

Sample no.	GFZ sample no.	TEM sample no.	Stylolite	Carbonate type of host rock	Organic matter type	Thermal maturity of organic matter	Vitrinite reflectance R_r (%)
Chalk-1a	G015404	4361	Horizontal, upper part	Calcite	II	Early oil window	~0.5%
Chalk-1b	G015405	4352	Horizontal, lower part	Calcite	II	Early oil window	~0.5%
Schaumkalk-1a	G015500	4282	Horizontal	Calcite	II (III?)	Early oil window	~0.6% (T_{max}: 436°C)
Schaumkalk-2a	G015502	4284	Horizontal	Calcite	II (III?)	Early oil window	~0.6% (T_{max}: 436°C)
Ca2-1a	G015406	4082	Horizontal	Dolomite	II	Immature	~0.4–0.5% (T_{max}: 420°C)
Ca2-1b	G015407	4089	Perpendicular	Dolomite	II	Immature	~0.4–0.5% (T_{max}: 420°C)
Ca2-1c	G015408	4178	Coarse-grained matrix	Dolomite	II	Immature	~0.4–0.5% (T_{max}: 420°C)
Ca2-1d	G015409	4176	Fine-grained matrix	Dolomite	II	Immature	~0.4–0.5% (T_{max}: 420°C)
Ca2-2	G015410	4321	Horizontal	Dolomite	II	Dry gas generation	>1.5%
Ca2-3	G015412	4319	Horizontal	Dolomite	II	Oil window	~1.0%
Ca1-1a	G015416	4253	Horizontal	Calcite	II	Oil window	~0.8%
Ca1-1b	G015417	4244	Perpendicular	Calcite	II	Oil window	~0.8%
Ca1-2a	G015418	4257	Horizontal	Calcite	II	Oil window	~0.8%
Ca1-2b	G015419	4255	Perpendicular	Calcite	II	Oil window	~0.8%

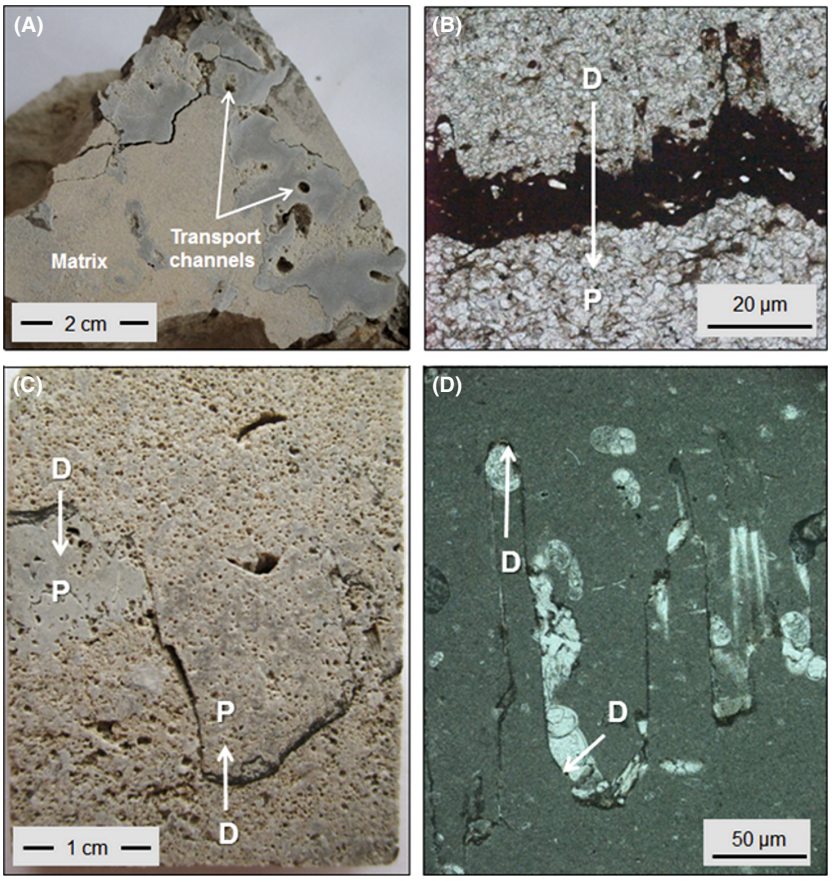

Fig. 2. Stylolite appearance in the investigation material – part 1. (A) Open channels for transport of dissolved ions. The channels are surrounded by tightened grey carbonate areas. Sample Schaumkalk-1a. View on bedding plane. (B) Tightened areas due to precipitation (P) below the stylolite interfaces and dissolution (D) above. Sample Schaumkalk-2a. (C) Tightened areas due to precipitation (P) above or below the stylolite interfaces. Sample Schaumkalk-2a. (D) Obvious concentration of microfossil remnants above and below stylolites in North Sea Chalk sample 1.

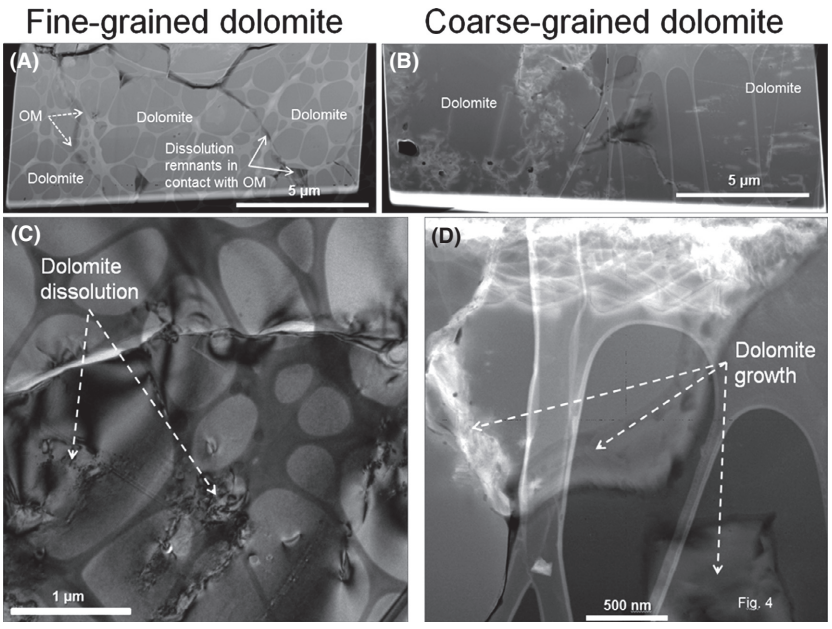

Fig. 3. Sample Ca2-1. Locations of focused ion beam (FIB) sections are presented in Fig. 2B. High-magnification scanning transmission electron microscopy (STEM) images (high-angle annular dark-field [HAADF] mode) showing fine-grained dolomite matrix (A) and coarse-grained dolomite (B). TEM Bright Field images demonstrate dissolution of dolomite in the fine-grained matrix above the stylolite (Fig. 4C), and dolomite growth in the coarse-grained matrix underlying the stylolite (Fig. 4D).

tightened parts are composed of coarser-grained carbonate cement (Fig. 3B,D). In contrast, fine-crystalline carbonate parts underwent dissolution (Figs 2B and 3A,C). In the investigated samples, stylolite formation is independent on carbonate type and lithology, and occurs in calcite (Fig. 2A,D) and dolomite (Fig. 2B,C). Interface features at stylolites can be observed and are obvious when coccolithophorides in Chalk get concentrated due to larger

calcite crystals whereas the matrix made up of small calcite crystals dissolved. The coccolithophoride particles are only partly dissolved (Fig. 2D). However, dissolution in the investigated Chalk sediments can occur above and below the clayey stylolite (Fig. 2D). Different interface reactions above and below a stylolite are well developed in the Ca1 carbonate in Luckenwalde (overview in Fig. 4A). In this example, dissolution took place above the stylolite with open pore space towards the overlying dissolved carbonate (Fig. 4C), whereas an intact interface without carbonate corrosion is maintained below the stylolite (Fig. 4B). However, open and vertical pore space in the form of channels can be also preserved in the centre of stylolites from the Schaumkalk (Fig. 2A).

In stylolites, many features caused by organic–inorganic interactions can be observed at the direct interface to organic matter (Fig. 5). For example, initially precipitated pyrite is surrounded by siderite ribbons (Fig. 5B), or pyrite and siderite are intimately intergrown (Fig. 5D). Besides their occurrence as single grains (Fig. 5E), TiO_2 polymorphs can also occur as agglomerates of nanocrystals (Fig. 5F). Clay minerals in stylolites are partly detrital (Fig. 5A,B) or authigenic, and the latter can have an interface with organic matter in the stylolite (Fig. 5C). However, in all organic matter-bearing stylolites open pores exist both between minerals (e.g. Fig. 5D,E) and also in organic matter (Fig. 5C).

An exceptional stylolite formation due to different calcite crystal sizes is recorded in the Chalk sediments which is characterized by the concentration of partly corroded microfossils (Fig. 2D). Precipitation of exclusively micrometre-sized calcite crystals took place above and below the stylolite (precipitation above the stylolite demonstrated in Fig. 6E) whereas below the stylolite a loosely packed matrix of coccolithophoride fragments prevails (Fig. 6D). This difference could have also prevailed prior to stylolitization as stylolites have been suggested to develop along textural discontinuities. However, corrosion or precipitation of carbonate in the Chalk samples is focussed to the direct stylolite contact, and not observable in a distance of millimetres from the clayey stylolite (Fig. 6B,C).

Hydrogeochemical modelling

To simulate calcite dissolution under a variety of different pressure (P) and temperature (T) conditions, different scenarios have been calculated. The scenarios cover the P/T conditions from 30 bar/75°C to 80 bar/300°C (Fig. 6), and consider the approximate P/T conditions in a sedimentary basin under hydrostatic conditions. Three different scenarios have been calculated for the conceptual addition of 0.1, 1.0, and 10.0 moles of OMP.

In scenario 1, the addition of 0.1 OMP moles into the generic reactor does not cause significant calcite dissolution (Fig. 7A). At 30°C 0.1 mmoles calcite is dissolved and dissolution increases to 0.3 mmoles at 80°C at 300 bar. The low calcite solubility is coupled to a pH stability of 5.2–5.3 of the aqueous solution. The $CO_{2(gas)}$ concentrations in

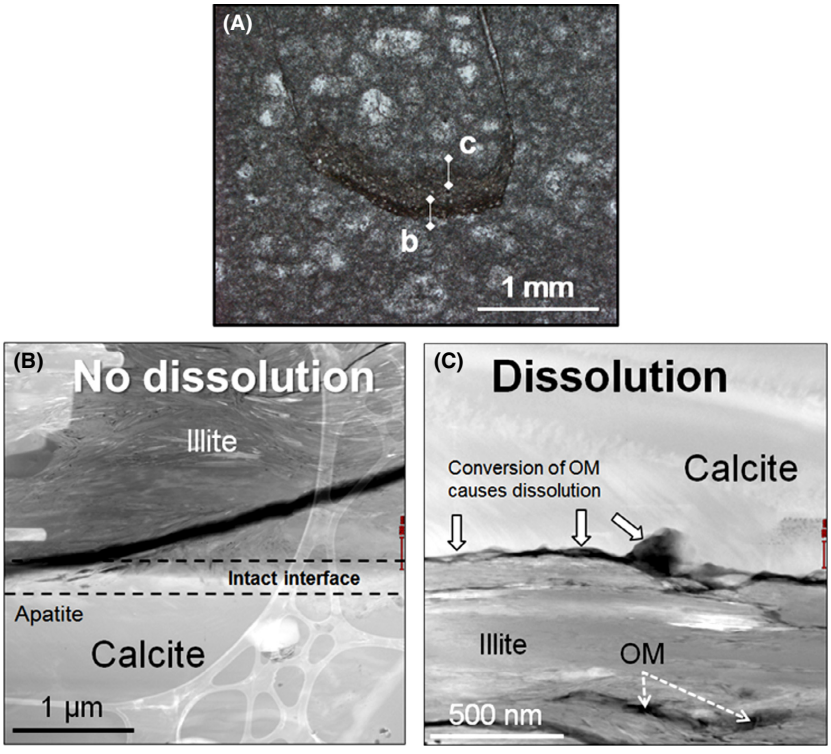

Fig. 4. Optical micrograph of sample Ca1-2 with location of FIB sections (b, c) (A). The high-magnification scanning transmission electron microscopy (STEM) images (high-angle annular dark-field [HAADF] mode) show dissolution on the upper side of the stylolite (C), whereas an intact interface occurs at the lower side (B).

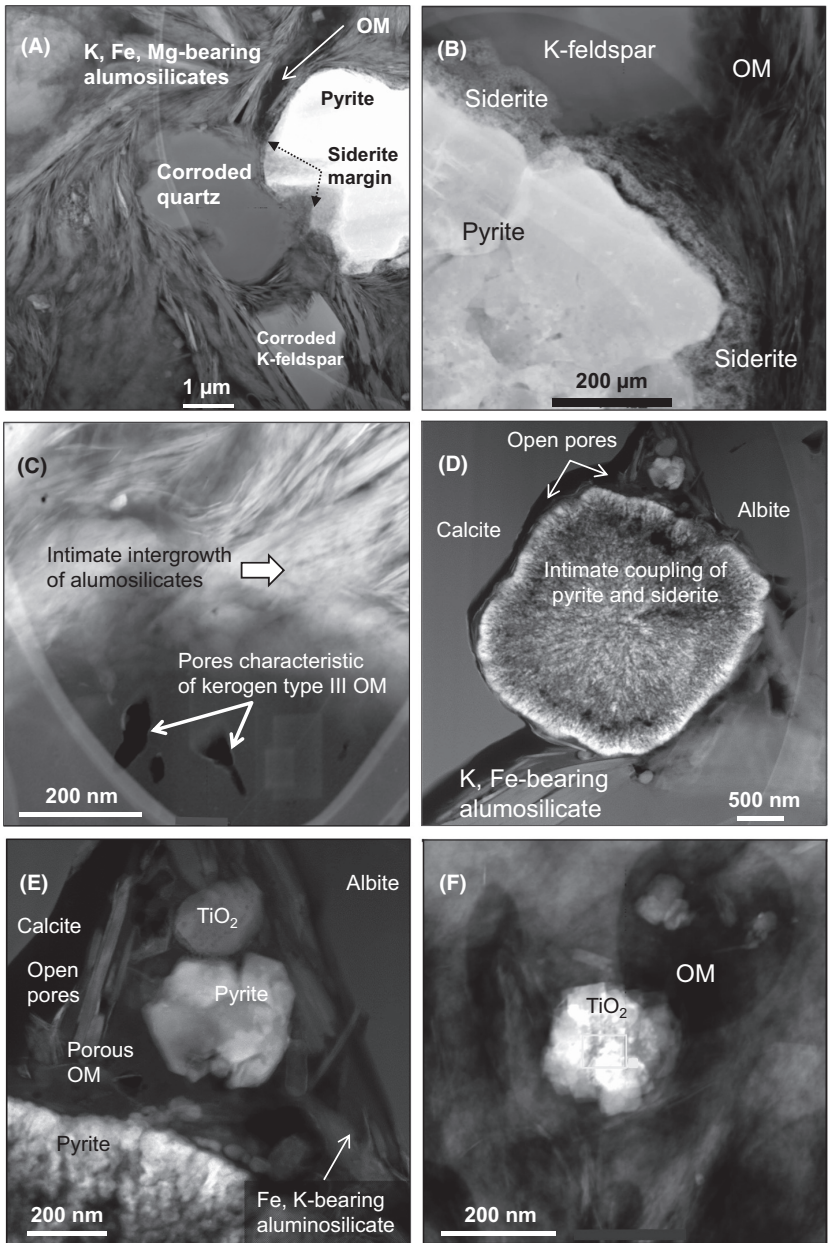

Fig. 5. High-magnification scanning transmission electron microscopy (STEM) images (high-angle annular dark-field [HAADF] mode) about complex mineral reactions in stylolites due to conversion of organic matter. Pyrite with siderite margin occurs in clayey matrix together with obvious corrosion of quartz and K-feldspar, and authigenesis of clay minerals; sample Schaumkalk-1a (A). Details about the stylolite in sample Schaumkalk-1b pyrite (B) show pyrite crystals surrounded by a siderite ribbon, and K-feldspar corrosion in direct contact to organic matter. A direct interface of porous organic matter (OM) and growing clay minerals; sample Schaumkalk-1a (C). A further direct interface between the stylolite and the carbonate host matrix demonstrates processes in a porous interface where a pyrite–siderite nodule grew and where albite corrosion took place in sample Ca2-2 (D). In the stylolite of sample Ca2-2, porosity is high, and porous organic matter occurs besides a nonagglomerated titania crystal (E). In contrast, agglomerated titania polymorphs occur in sample Schaumkalk-1b and indicate low pH (F).

the generic reactor remain fairly constant, and a dissolution from 0.1 to 0.3 mmoles occurs during increasing *P*, *T*-conditions.

In Scenario 3, the addition of 10 moles of OMP is simulated (Fig. 7C). From 40°C/100 bar on calcite is progressively dissolved from 1.6 to 5.8 mmoles at 80°C at 300 bar. In contrast to scenario 1, pH is lower and slightly decreases from 4.9 at 30°C/75 bar to 4.7 at 80°C/300 bar. In contrast to scenario 1, the $CO_{2(gas)}$ levels in the generic are higher, and increase from 3.0 to 17.3 moles (with constant low dissolution rates from 3 to 17.3 mmoles of CO_2).

In scenario 2, 1.0 mol of OMP is added to the generic reactor (Fig. 7B). At a temperature between 30–35°C and at 75 bar, calcite is relatively stable (dissolution of around 1 mmoles of calcite). There is a break at 40°C and 100 bar when 29 mmoles calcite dissolve. With increasing temperature and pressure, calcite dissolution remains high (24 mmoles at 80°C/300 bar). In contrast to scenario 3 (Fig. 7C), the $CO_{2(gas)}$ concentrations are lower and increase slightly from 2.4 to 5.3 moles during increasing *P*, *T* from 40°C/100 bar to 80°C/300 bar.

DISCUSSION

In general, stylolite development is dependent on the carbonate type, and seems to be more developed (higher amplitudes and thickness) in limestone than in dolomite

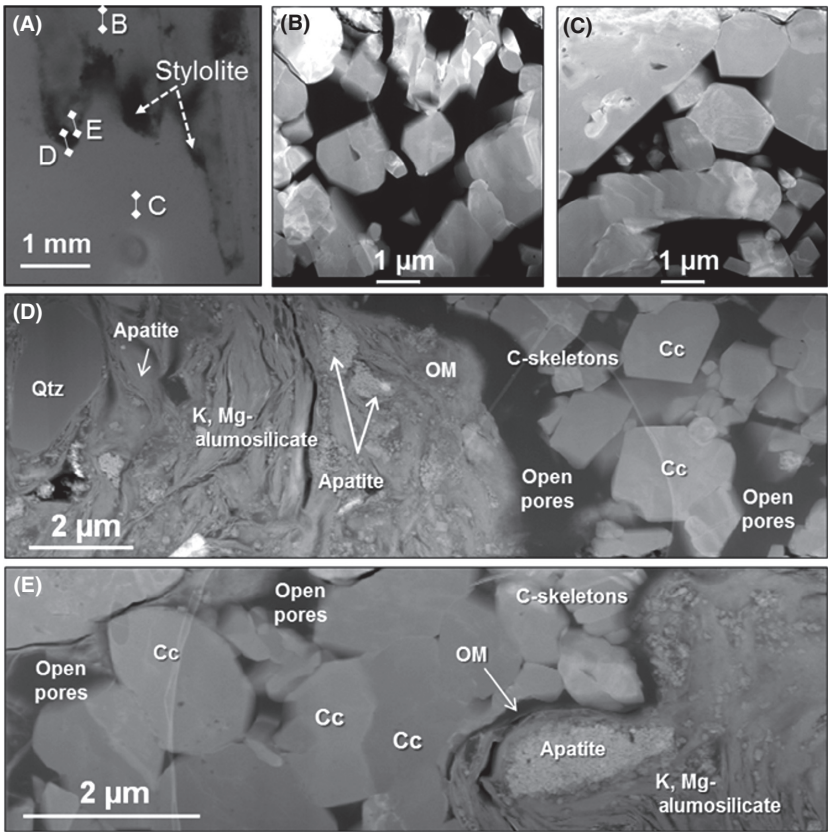

Fig. 6. Thin section microscope image of Chalk-1 sample (A) showing stylolite with locations of FIB sections (B, C, D, E). FIB sections show high-magnification scanning transmission electron microscopy (STEM) images (high-angle annular dark-field [HAADF] mode). (B, C) A high porosity prevails above and below the clayey stylolite interface. Calcite crystals appear not corroded, and fossilized coccolithophoride skeleton particles are preserved. Below the stylolite (D), calcite crystals appear noncorroded and high porosity prevails. Less porosity occurs above the stylolite (E) and calcite crystals appear amalgamated due to calcite precipitation, and remnants of coccolithophoride skeletons occur at the direct contact to the stylolite.

(Peacock & Azzam 2006). Moreover, carbonate texture is assumed to play a major control as more serrate stylolites are reported from grainstones and packstones in contrast to wackestones and mudstones (Friedel 1995; Andrews & Railsback 1997). The investigated stylolites in this study occur both in limestone and in dolomite, and similarly serrated stylolites occur in mudstones such as Chalk or the Schaumkalk. However, all stylolites contain organic matter of variable amounts, type and thermal maturity.

Organic matter-bearing stylolites occur in all investigated samples with thermal maturities from immature conditions to the dry gas window (Table 2). Accordingly, stylolitization controlled by the release of OMP can start already at thermal maturities of around 0.4% R_r, and is considered to decrease with ongoing burial as the solubility of calcite and other carbonate minerals is retrograde with respect to temperature (Bjørlykke & Jahren 2012; Coto *et al.* 2012). From early diagenesis to the beginning of the oil window, organic matter is converted into CO_2, CH_4, H_2 (Carr & Williamson 1990; Payne & Ortoleva 2001a,b), significant amounts of water (Vandenbroucke & Largeau 2007), and acetic acid (and other LMWOAs, such as oxalic acid; see also, e.g. Tissot *et al.* 1974; Surdam *et al.* 1989; Seewald 2003). A generalized sketch summarizing these processes is presented in Fig. 8 as a H/C versus O/C diagram of the atomic ratios. Accordingly, the diagenetic processes create acidic and corrosive aqueous fluids (ACF) which can dissolve carbonate (van Berk *et al.* 2015), especially at low thermal maturities.

The released compounds are especially formed by terrestrial organic matter (kerogen type III), but also by marine organic matter (kerogen type II), and these generation processes are reflected by the strong decrease of the atomic O/C ratio until a thermal maturity of around 0.5% R_r (Fig. 8) is achieved. Especially kerogen type III organic material releases ACF over a broader maturity interval (also beyond 0.5% R_r). The loss of, for example, oxygen in the form of CO_2 (10–105 mg CO_2/g TOC) has been quantified using a natural maturity series of coals from New Zealand (R_r = 0.2–0.8%; Vu *et al.* 2013), and the progressive elimination of the C=O groups from ester and ketone groups is regarded as the main reason (Rouxhet & Robin 1978). Additionally, many different low molecular weight compounds have been detected by analytical pyrolysis to simulate thermal degradation of kerogen (summarized in Horsfield *et al.* 2006). It is furthermore important for the interpretation of the results of this study to consider that also acetate and acetic acid are generated from kerogens during hydrous pyrolysis (Barth *et al.* 1989). Theoretical considerations (which probably not reflect natural processes) also point to water generation from kerogen (Fig. 8). As water is needed for organic–inorganic

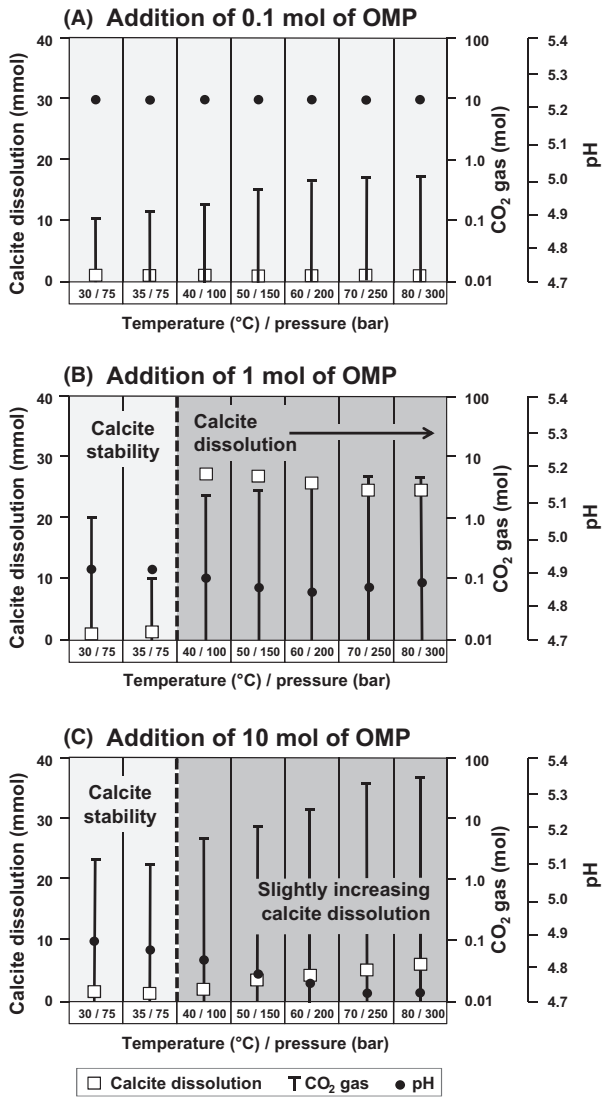

Fig. 7. Results of the conceptual modelling approach about the release of kerogen maturation products (KMP) forming acidic and corrosive aqueous fluids (ACF) and causing calcite dissolution at variable temperature and pressure conditions similar to hydrostatic conditions in a sedimentary basin. To simulate calcite dissolution in a sedimentary basin, three different scenarios have been calculated for the conceptual addition of 0.1 mole (Fig. 6A), 1.0 mole (Fig. 6B) and 10.0 moles (Fig. 6C) of kerogen maturation products (KMP) into the generic modelling reactor. In each scenario, the calculations have been carried out considering variable *p*, T conditions which range from 30 bar/75°C to 80 bar/300°C. In scenario 1 and 3, the respective addition of 0.1/10 moles KMP into the generic reactor does not cause significant calcite dissolution independent on temperature and pressure. In scenario 2, the addition of 1.0 mole of KMP initiates an increased calcite dissolution at 40°C and 100 bar when 29 mmoles calcite dissolves. With increasing temperature and pressure in scenario 2, calcite dissolution remains high (24 mmoles at 80°C/300 bar). A balanced input of 1 mole KMP causes the suitable conditions for calcite dissolution.

rock–fluid interactions, this self-reinforcing process is mandatory for the availability of a water matrix for geochemical reactions, and may lead to fluids with a high dissolution potential against carbonate.

Clay minerals are also considered to precipitate in stylolites (Meike & Wenk 1988; Paganoni *et al.* 2016). Similar phenomena have been observed, for example, in the investigated Schaumkalk samples (e.g. Fig. 5C). In this example, new potassium-bearing aluminosilicate with low Mg contents is intimately intergrown with organic matter. Corroded K-feldspar (Fig. 5B) is considered to be due to the activity of ACF sourced from the organic matter, and points to a major control of clay minerals for stylolite formation (e.g. Bjørlykke & Jahren 2012). Besides the hypothesis that clay minerals in stylolites are residues left by the dissolution of clay-bearing carbonate, one further consideration refers to a more active control of clay minerals as catalysts for dissolution. This consideration is based on the fact that H_2O molecules may provide a water film surrounding clay particles which might enable pathways for diffusion of ions (Weyl 1959).

Dissolution of carbonate causes disequilibria of stable rock–fluid systems and mass transfer either by migration of aqueous solutions enriched in ions or by diffusion (dependent on the permeability of the system). Safaricz & Davison (2005) suggested strong fluid flows to transport the dissolved solids ('open pressure-solution system'), and calculated a thirty-fold volume dissolution to create stylolites in Cretaceous to Palaeogene North Sea Chalk (see highly porous Chalk sediments in Fig. 6B,C). In contrast, calculations by Bjørlykke & Jahren (2012) showed that after burial to a depth without meteoric water inflow (and without hydrothermal convection), the bulk chemical composition of a carbonate sediment remains constant due to limited pore water flow. The authors, furthermore, stated that thin clay laminae and stylolites limit the flow perpendicular to bedding and by diffusion. The presented FIB-TEM results demonstrate that porosity prevails within the stylolite and along its boundaries (Figs 4–6) and that aqueous fluids enriched with ions from carbonate dissolution can be transported. In any case, the presence of formation water is essential as a hydrogeochemical reactor for dissolution. In contrast, carbonate dissolution is argued to be retarded or completely depressed due to hydrocarbon filling, for example leading to porosity preservation in chalk. Two potential factors probably can cause this effect: (i) slow diffusion in the water phase or (ii) the adsorption of polar hydrocarbons to the calcite surface (Fabricius 2007).

A minimum depth to cause carbonate dissolution for stylolitization is still a matter of debate and has been reported, for example, from 90 m depth (Schlanger *et al.* 1964), 500 m deep Chalk sediments in the Caribbean Sea (Fabricius 2007) and 600–900 m deep carbonate reservoirs in the Middle East (Dunnington 1967). In general, carbonate dissolution decreases with temperature, but increases with pressure (e.g. Coto *et al.* 2012). In this study, the temperature dependence of calcite solubility was simulated by hydrogeochemical modelling the processes at

an interface between a TOC-bearing clayey layer and a carbonate matrix. Accordingly, carbonate dissolution is thermodynamically favoured at temperatures exceeding at least 40°C (Fig. 7B) which corresponds to a depth of <800 m assuming a geothermal gradient of 30°C/km and a mean surface temperature of 20°C. As mean surface temperatures during earth history temporarily may have been significantly higher, a lower depth for the onset of stylolitization can be assumed. However, this result is in agreement with observations that stylolites are rare in carbonate rocks which have not reached the thermal maturity of the early oil window (around 0.5% R_r) during their burial history. Thus, pressure due to burial depth might be a factor, but the release of water during the pre- and early oil window is an additional important factor as it forms the actual matrix for the dissolution of acidic and corrosive compounds, and as a reactor for such processes. In all calculated hydrogeochemical scenarios, 45 ml of H_2O is generated (results not presented), points to a self-reinforcing process for stylolitization and supports the suggested hypothesis that water is an essential factor. However, a major finding of the modelling results is that a clayey layer which is the reactor for the release of water and soluble low molecular compounds must contain a specific and balanced TOC content to cause strong calcite dissolution. It was demonstrated by the modelling approach that 1 mol of OMP causes strongest calcite dissolution at temperatures exceeding 40°C and pressures higher than 75 bar (Fig. 7B). Less calcite dissolution may be due to (i) relatively higher pH of the pore water (at lower TOC contents), or (ii) less CO_2 solubility (due to conversion of higher TOC contents).

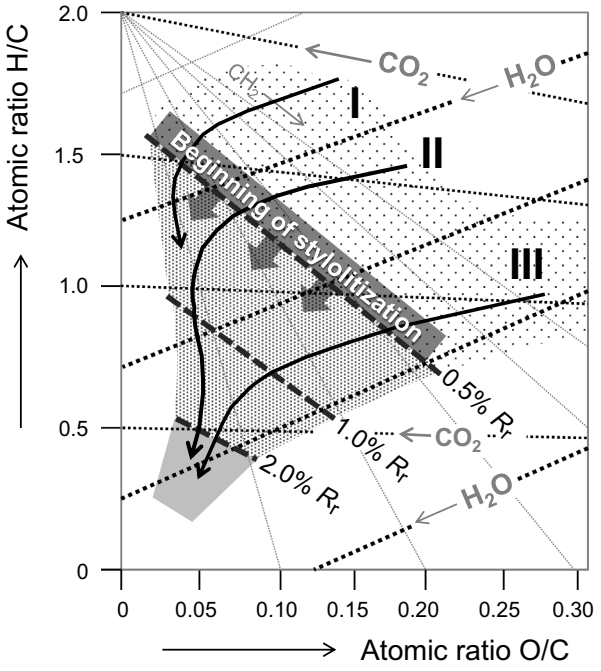

Fig. 8. General scheme showing the evolution of the atomic H/C and O/C ratios for different kerogen types I, II and III during maturation (redrawn after Tissot & Welte 1984). Until hydrocarbon generation at approximately 0.5% R_r, the organic material mainly dewaters and releases significant portions of CO_2. This process continues for kerogen type III until approximately 1.0% R_r. Conceptually, carbonate can be dissolved during this phase leading to clayey residues forming stylolites (red stylolitization window) as water as a matrix for geochemical processes is available and also soluble carbon dioxide which may lower pH. Carbon dioxide in this diagram also represents oxygen-bearing compound classes such as acids (e.g. acetic acid) which may be regarded as soluble corrosive and acidic components. The evolution path of the different kerogen types parallel to the *y*-axis and to lower H/C ratios relates to the predominant release of hydrocarbons.

The onset and end of oil generation (oil window) are dependent on the organic matter type. For example, type II kerogen (marine organic matter) releases C_{6-14} hydrocarbons in a maturity window between 0.6 and 1.3% R_r, whereas nonhydrocarbons are released earlier (e.g. Stainforth 2009). The maturity interval around 0.5% R_r relates approximately to subsurface temperatures of 60°C. Lower temperatures of around 40°C, however, are suggested as the transition temperature towards higher calcite solubility in the generic hydrogeochemical interface model (Fig. 7B). In summary, the temperature of 40°C (approximately 0.4%

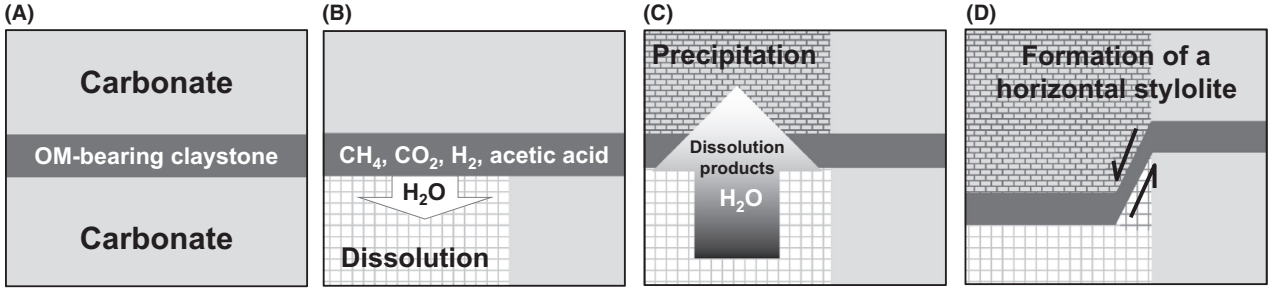

Fig. 9. Conceptual model about the formation of a horizontal stylolite in carbonate rocks due to the release of aqueous acidic and corrosive maturation products of organic matter during the pre-oil window. (A) Situation before the release of pre-oil acidic and corrosive fluids from the organic matter-bearing claystone. (B) Release of an aqueous fluid enriched in methane, carbon dioxide, molecular hydrogen and acetic acid. The underlying carbonate is dissolved. (C) Dissolved products of carbonate dissolution are transported upward by diffusion or by migration along permeable conduits and cause precipitation of carbonate. (D) Final stage of the stylolite formation process.

vitrinite reflectance, R_r) is the temperature threshold value above which stylolite formation in carbonate rocks can be stimulated due to the release of aqueous nonhydrocarbons. However, also terrestrial organic matter (kerogen type III) is capable of supporting stylolite formation in carbonates, but is generally rare due to depositional conditions. Kerogen type III organic matter – in contrast to type II – generates predominantly nonhydrocarbons (Cooles *et al.* 1987) and is thus better suited to support stylolitization in carbonates.

Carbonate reservoir rocks with locally increased porosity are described, for example, from the Middle East (Melville *et al.* 2004; Lambert *et al.* 2006). Theoretical considerations implemented in hydrogeochemical models came to the result that such locally enhanced porosity can be result of acidic fluids that migrated as a pre-oil phase through the reservoir (van Berk *et al.* 2015). These aqueous fluids have an acidic and corrosive character and may cause calcite dissolution along their migration path following a decreasing pressure and temperature regime. In contrast, processes in stylolites and at their interfaces to the lower and upper carbonate matrix operate at much smaller dimensions which is due to the thinner clay layers and lower TOC amounts. Accordingly, these small 'black shales' release only few aqueous solutions which are capable of creating localized porosity leading to precipitation at the opposite side.

CONCLUSIONS

The irreducible mineralization of organic matter is suggested to be an important controlling factor for the development of stylolites in carbonate rocks (Fig. 9).

The maturation of organic matter leads to the release of an aqueous phase enriched in soluble CO_2, CH_4, acetic acid and further LMWOAs. This aqueous solution has an acidic and corrosive character due to its low pH and – after expulsion – is capable to dissolve carbonate such as calcite or dolomite at a temperature of approximately 40°C, which may correspond to a depth of <800 m under hydrostatic conditions (given a geothermal gradient of 30°C and a surface temperature of 20°C). Water that is also released during maturation of organic matter acts as reactant, solvent and matrix for the hydrogeochemical processes of carbonate dissolution and precipitation.

The clayey matrix of serrated stylolites in carbonates is considered to be a micro-environment in which complex organic–inorganic rock–fluid interactions take place. These interactions are driven by the presence of water and its dissolved contents, and are finally mini-reactors in which triggered thermodynamic instabilities tend to equilibrium. The migration of the aqueous phase may be channelled in narrow tubes or along conduits with sufficient interconnected porosity and permeability, or by diffusion. This process may result in localized carbonate dissolution, and the dissolved ions precipitate nearby to balance this disequilibrium.

In the clayey matrix, mineral phases such as quartz or feldspar may be corroded due to the changed hydrogeochemical conditions (pH) and may lead to clay mineral precipitation in close and genetic relationship to organic matter.

All these processes require the generation of water from organic matter maturation. However, during maturation, also CO_2, CH_4, and LMWOAs are generated. These maturation-dependent processes already take place during early diagenesis at shallow depth, but are intensified during the stage of pre-oil generation. The investigated sample suite has left the early diagenetic stage and is – at minimum – at the beginning of the oil window and beyond. Accordingly, the described processes are one key factor besides hydrostatic pressure, and only the interacting combination of both factors is finally capable to cause carbonate dissolution leading to horizontal stylolitic structures in carbonate rocks. Similar processes can take place in sandstones with clayey, OM-bearing intercalations leading to the generation of corrosive and acidic aqueous fluids which cause dissolution of quartz, feldspar and other reactive minerals. And last, but not least stylolitization by comparable processes can also occur in vertically oriented, permeable conduits in carbonates leading to vertical stylolites.

ACKNOWLEDGEMENTS

The authors are grateful to Karsten Obst (LUNG, Schwerin, Germany), Michael Göthel (LBGR, Wünsdorf, Germany), Niels H. Schovsbo (GEUS, Copenhagen, Denmark), Uwe Schridde (Rump & Salzmann, Osterode, Germany) and Andreas Koszinski (CEMEX OstZement GmbH, Rüdersdorf, Germany) to providing material for investigations. W. van Berk (Clausthal-Zellerfeld, Germany) is gratefully acknowledged for supporting modelling. We also thank two anonymous reviewers for the critical comments and constructive suggestions, and G. Etipoe for the editorial handling of the manuscript.

REFERENCES

Alsharhan AS, Sadd J (2000) Stylolites in Lower Cretaceous carbonate reservoirs, UAE. *Society for Sedimentary Geology Special Publication*, **69**, 185–207.

Andrews LM, Railsback LB (1997) Controls on stylolite development: morphologic, lithologic, and temporal evidence from bedding-parallel and transverse stylolites from the U.S. Appalachians. *The Journal of Geology*, **105**, 59–73.

Arning ET, Fu Y, van Berk W, Schulz H-M (2011) Organic carbon remineralisation and complex, early diagenetic solid–aqueous solution–gas interactions: case study ODP Leg 204, Site 1246 (Hydrate Ridge). *Marine Chemistry*, **126**, 120–31.

Barth T, Borgund AE, Hopland AL, Graue A (1988) Volatile organic acids produced during kerogen maturation— amounts, composition and role in migration of oil. *Organic Geochemistry*, **13**, 461–5.

Barth T, Borgund AE, Hopland AL (1989) Generation of organic compounds by hydrous pyrolysis of Kimmeridge oil shale – bulk results and activation energy calculations. *Organic Geochemistry*, **14**, 69–76.

Bäuerle G, Bornemann O, Mauthe F, Michalzik D (2000) Origin of stylolites in Upper Permian Zechstein anhydrite (Gorleben Salt Dome, Germany). *Journal of Sedimentary Research*, **70**, 726–37.

van Berk W, Fu Y, Schulz H-M (2015) Creation of pre-oil-charging porosity by migration of sourcerock-derived corrosive fluids through carbonate reservoirs: onedimensional reactive mass transport modelling. *Petroleum Geoscience*, **21**, 35–42.

Bjørlykke K, Jahren J (2012) Open or closed geochemical systems during diagenesis in sedimentary basins: constraints on mass transfer during diagenesis and the prediction of porosity in sandstone and carbonate reservoirs. *AAPG Bulletin*, **96**, 2193–214.

Carr AD, Williamson JE (1990) The relationship between aromaticity, vitrinite reflectance and maceral composition of coals: implications for the use of vitrinite reflectance as a maturation parameter. *Advances in Organic Geochemistry*, **16**, 313–23.

Cooles GP, Mackenzie AS, Parkes RJ (1987) Non-hydrocarbons of significance in petroleum exploration: volatile fatty acids and nonhydrocarbon gases. *Mineralogical Magazine*, **51**, 483–93.

Coto B, Martos C, Pena JL, Rodríguez R, Pastor G (2012) Effects in the solubility of CaCO3: experimental study and model description. *Fluid Phase Equilibria*, **324**, 1–7.

Dunham JB, Larter S (1981) Association of stylolitic carbonates and organic matter: implications for temperature control on stylolite formation (abs.). *AAPG Bulletin*, **65**, 922.

Dunnington HV (1967). Aspects of diagenesis and shape change in stylolitic limestone reservoirs. *Mexico: 7th World Petroleum Congress Proceedings*, **2**, 339–52.

Fabricius IL (2007) Chalk: composition, diagenesis and physical properties. *Bulletin of the Geological Society of Denmark*, **55**, 97–128.

Friedel C-H (1995) Stylolithen im Rüdersdorfer Schaumkalk – Wechselwirkung zwischen sedi-mentären Gefüge und Spannung. *Berliner geowissenschaftliche Abhandlungen, A*, **168**, 219–35.

Fu Y, van Berk W, Schulz H-M (2016) Hydrogen sulfide formation, fate, and behavior in anhydrite-sealed carbonate gas reservoirs: a three-dimensional reactive mass transport modeling approach. *AAPG Bulletin*, **100**, 843–65.

Gao G, Hao S, Wang H (1999) Characteristics of hydrocarbon generation and expulsion in matrix and stylolite of carbonate rocks. *Science in China Series D*, **42**, 202–6.

Hofmann P, Leythaeuser D (1995) Migration of hydrocarbons in carbonate source rocks of the Staßfurt member (Ca2) of the Permian Zechstein, borehole Aue 1, Germany: the role of solution seams. *Organic Geochemistry*, **23**, 597–606.

Horsfield B, Schenk HJ, Zink K, Ondrak R, Dieckmann V, Kallmeyer J, Mangelsdorf K, di Primio R, Wilkes H, Parkes RJ, Fry J, Cragg B (2006) Living microbial ecosystems within the active zone of catagenesis: implications for feeding the deep biosphere. *Earth and Planetary Science Letters*, **246**, 55–69.

Lambert L, Durlet C, Loreau JP, Marnier G (2006) Burial dissolution of micrite in Middle East carbonate reservoirs (Jurassic–Cretaceous): keys for recognition and timing. *Marine and Petroleum Geology*, **23**, 79–92.

Leythaeuser D, Borromeo O, Mosca F, di Primio R, Radke M, Schaefer RG (1995) Pressure solution in carbonate source rocks and its control on petroleum generation and migration. *Organic Geochemistry*, **12**, 717–33.

Lind IL (1993) Stylolites in chalk from Leg 130, Ontong Java Plateau. *Proceedings of the Ocean Drilling Program, Scientific Results*, **120**, 445–51.

Lorant F, Behar F (2002) Late generation of methane from mature kerogens. *Energy & Fuels*, **16**, 412–27.

Lundegard PD, Land LS (1989) Carbonate equilibria and pH buffering by organic acids – response to changes in p_{CO2}. *Chemical Geology*, **74**, 277–87.

Mazzullo SJ, Harris PM (2009) An overview of dissolution porosity development in the deep-burial environment, with examples from carbonate reservoirs in the Permian Basin. In: *Permian Basin Plays – Tomorrow's Technology Today*, vol. 91-89 (ed. Candelaria M), pp. 125–38. West Texas Geological Society (and Permian Basin Section SEPM), Midland, TX, USA.

Meike A, Wenk H-R (1988) A TEM study of microstructures associated with solution cleavage in limestone. *Tectonophysics*, **154**, 137–48.

Melville P, Al Jeelani O, Al Menhali S, Grötsch J (2004) Three-dimensional seismic analysis in the characterization of a giant carbonate field, onshore Abu Dhabi, United Arab Emirates. In: *Seismic Imaging of Carbonate Reservoirs and Systems*, vol. 81 (eds Eberli GP, Massaferro JL, Sarg RF), pp. 123–48. American Association of Petroleum Geologists, Memoirs, Tulsa, Oklahoma.

Metcalf AS, Parker CP, Boles JL (2005) Acetic acid demonstrates greater carbonate dissolution than typically expected. *Journal of Canadian Petroleum Technology*, **44**, 22–4.

Moore CH, Wade WJ (2013) Chapter 10 - Burial diagenetic environment. In: *Developments in Sedimentology*, vol. 67 (eds Moore CH, Wade WJ), pp. 239–84. Elsevier, Amsterdam.

Nenna F, Aydin A (2011) The formation and growth of pressure solution seams in clastic rocks: a field and analytical study. *Journal of Structural Geology*, **33**, 633–43.

Nicolaides S, Wallace MW (1997) Pressure-dissolution and cementation in an Oligo-Miocene non-tropical limestone (Clifton Formation), Otway Basin, Australia. In: *Cool-Water Carbonates*, vol. 56 (eds James NP, Clarke JAD), pp. 249–61. Society of Economic Paleontologists and Mineralogists Special Publication, Tulsa, Oklahoma.

Paganoni M, Al Harethi A, Morad D, Morad S, Ceriani A, Mansurbeg H, Al Suwaidi A, Al-Aasm IS, Ehrenberg SN, Sirat M (2016) Impact of stylolitization on diagenesis and reservoir quality: a case study from an early cretaceous reservoir in a giant oilfield, Abu Dhabi, United Arab Emirates. *Sedimentary Geology*, **335**, 70–92.

Parkhurst DL, Appelo CAJ (2013) Description of Input and Examples for PHREEQC Version 3—A Computer Program for Speciation, Batch-Reaction, One-Dimensional Transport, and Inverse Geochemical Calculations. In: *U.S. Geological Survey Techniques and Methods* (eds Salazar K, McNutt MK), book 6, chap. A43, 497 p. US. Department of the Interior, U.S. Geological Survey, Denver CO.

Payne DF, Ortoleva PJ (2001a) A model for lignin alteration. Part 1. A kinetic reaction-network model. *Organic Geochemistry*, **32**, 1073–85.

Payne DF, Ortoleva PJ (2001b) A model for lignin alteration. Part II. Numerical model of natural gas generation and application to the Piceance Basin, Western Colorado. *Organic Geochemistry*, **32**, 1087–101.

Peacock DCP, Azzam IN (2006) Development and scaling relationships of a stylolite population. *Journal of Structural Geology*, **28**, 1883–9.

Peryt TM, Orti F, Rosell L (1993) Sulfate platform-basin transition of the lower Werra Anhydrite (Zechstein, Upper Permian), western Poland; facies and petrography. *Journal of Sedimentary Petrology*, **63**, 646–58.

Petersen HI, Nytoft HP, Vosgerau H, Andersen C, Bojesen-Koefoed JA, Mathiesen A (2010) Source rock quality and maturity and oil types in the NW Danish Central Graben: implications for petroleum prospectivity evaluation in an Upper Jurassic sandstone play area. In: *Petroleum Geology: From Mature Basins to New Frontiers* (eds Vining BA, Pickering SC), pp. 95–111. Proceedings of the 7th Petroleum Geology Conference, London, UK.

di Primio R, Leythaeuser D (1995) Quantification of the effect of carbonate redistribution by pressure solution in organic-rich carbonates. *Marine and Petroleum Geology*, **12**, 735–9.

di Primio R, Skeie JE (2004) Development of a compositional kinetic model for hydrocarbon generation and phase equilibria modelling: a case study from Snorre Field, Norwegian North Sea. In: *Understanding Petroleum Reservoirs. Towards an Integrated Reservoir Engineering and Geochemical Approach*, vol. 237 (eds Cubitt JM, England WA, Larter S), pp. 157–74. The Geological Society of London, Special Publications, Bath, UK.

Prochnow EA, Remus MVD, Ketzer JM, Gouvea JCR Jr, Schiffer de Souza R, De Ros LF (2006) Organic-inorganic interactions in oilfield sandstones: examples from turbidite reservoirs in the Campos Basin, Offshore eastern Brazil. *Journal of Petroleum Geology*, **29**, 361–80.

Railsback LB (1993) Lithologic controls on morphology of pressure-dissolution surfaces (stylolites and dissolution seams) in Paleozoic carbonate rocks from the mideastern United States. *Journal of Sedimentary Research*, **63**, 513–22.

Rouxhet PG, Robin PL (1978) Infrared study of the evolution of kerogens of different origins during catagenesis and pyrolysis. *Fuel*, **57**, 533–40.

Safaricz M, Davison I (2005) Pressure solution in chalk. *AAPG Bulletin*, **89**, 383–401.

Schlanger SO, Hathaway JC, Carroll D (1964) Petrology of the limestones of Guam, with a section on petrography of the insoluble residues. *Geological Survey Professional Paper*, **403-D**, 52.

Schretzenmayr S, Giesemann K, Höhlein A-C (1987) Katalog von Absenkungsdiagrammen der wichtigsten Rotliegendbohrungen in Ostbrandenburg. Report, 17 p., 29 Appendixes, Gommern (unpublished). In: Beer H, Stackebrandt W (2010) Zechstein – Paläomorphologie, Mächtigkeit und Tiefenlage. Atlas zur Geologie von Brandenburg, 4th edition. (ed. Landesamt für Bergbau, Geologie und Rohstoffe Brandenburg), pp. 82–3. Cottbus, Germany.

Seewald JS (2003) Organic–inorganic interactions in petroleum-producing sedimentary basins. *Nature*, **426**, 327–33.

Smith MM, Sholokhova Y, Hao Y, Carroll SA (2013) CO2-induced dissolution of low permeability carbonates. Part I: characterization and experiments. *Advances in Water Resources*, **62C**, 370–87.

Stainforth JG (2009) Practical kinetic modeling of petroleum generation and expulsion. *Marine and Petroleum Geology*, **26**, 552–72.

Surdam RC, Crossey LJ, Hagen ES, Heasler HP (1989) Organic-inorganic and sandstone diagenesis. *AAPG Bulletin*, **73**, 1–23.

Thomas AR, Dahl WM, Hall CM, York D (1993) $^{40}Ar/^{39}Ar$ analyses of authigenic muscovite, timing of stylolitization, and implications for pressure solution mechanisms; Jurassic Norphlet Formation, offshore Alabama. *Clays and Clay Minerals*, **41**, 269–79.

Tissot BP, Welte DH (1984) *Petroleum Formation and Occurrence*, 2nd edn. Springer Verlag, Berlin.

Tissot BP, Durand B, Espitalié J, Combaz A (1974) Influence of nature and diagenesis of organic matter in formation of petroleum. *AAPG Bulletin*, **58**, 499–506.

Vandenbroucke M, Largeau C (2007) Kerogen origin, evolution and structure. *Organic Geochemistry*, **38**, 719–833.

Von Bergen D, Carozzi AV (1990) Experimentally-simulated stylolitic porosity in carbonate rocks. *Journal of Petroleum Geology*, **13**, 179–92.

Vu TTA, Horsfield B, Mahlstedt N, Schenk HJ, Kelemen SR, Walters CC, Kwiatek PJ (2013) The structural evolution of organic matter during maturation of coals and its impact on petroleum potential and feedstock for the deep biosphere. *Organic Geochemistry*, **62**, 17–27.

Weyl PK (1959) Pressure-solution and the force of crystallization-A phenomenological theory. *Journal of Geophysical Research*, **64**, 2001–25.

Wirth R (2004) A novel technology for advanced application of micro- and nanoanalysis in geosciences and applied mineralogy. *European Journal of Mineralogy*, **16**, 863–76.

Wirth R (2009) Focused Ion Beam (FIB) combined with SEM and TEM: advanced analytical tools for studies of chemical composition, microstructure and crystal structure in geomaterials on a nanometre scale. *Chemical Geology*, **261**, 217–29.

APPENDIX

STEP 1 SCENARIO 1.0 MOLES OMP – 50DEGCELSIUS – 150 BAR

```
#---------------------- definition of additional
Acetate species from minteq.v4.dat
SOLUTION_MASTER_SPECIES
Acetate Acetate- 1.0 59.045 59.045
SOLUTION_SPECIES
Acetate- = Acetate-
 log_k 0
H+ + Acetate- = H(Acetate)
 log_k 4.757
 delta_h 0.41 kJ
 -gamma 0 0
 #         Id: 3309921
 #    log K source: NIST46.4
 #   Delta H source: NIST46.4
 #T and ionic strength: 0.00 25.0
Ca+2 + Acetate- = Ca(Acetate)+
 log_k 1.18
 delta_h 4 kJ
 -gamma 0 0
 #         Id: 1509920
 #    log K source: NIST46.4
 #   Delta H source: NIST46.4
 #T and ionic strength: 0.00 25.0
```

```
Na+ + Acetate- = Na(Acetate)
 log_k -0.18
 delta_h 12 kJ
 -gamma 0 0
 #         Id: 5009920
 #     log K source: NIST46.4
 #    Delta H source: NIST46.4
 #T and ionic strength: 0.00 25.0
K+ + Acetate- = K(Acetate)
 log_k -0.1955
 delta_h 4.184 kJ
 -gamma 0 0
 #         Id: 4109921
 #     log K source: NIST46.4
 #    Delta H source: NIST46.2
 #T and ionic strength: 0.10 25.0
SOLUTION 1
-pH 7.0 charge
-temp 50.0
-units mol/kgw
Cl 1.0
Na 1.0
REACTION_PRESSURE 1
150
EQUILIBRIUM_PHASES 1
Quartz 0.0 10
Kaolinite 0.0 10
Calcite 0.0 10
Anorthite 0.0 10
Albite 0.0 10
K-feldspar 0.0 10
SAVE solution 2
END
USE solution 2
EQUILIBRIUM_PHASES 2
Quartz 0.0 0.48
Kaolinite 0.0 0.48
Calcite 0.0 0.01
Anorthite 0.0 0.01
Albite 0.0 0.01
K-feldspar 0.0 0.01
REACTION_PRESSURE 2
150
REACTION 2
# OMP formation summarized by the overall reaction:
# R-CH2-CH2-CH3 + 4H2O = R + 2CO2 + CH4 + 5H2 (OMP);
Seewald (2003) and van Berk et al., 2009
CO2     1.9
CH4     0.9
H2      5.0
H(Acetate)  0.1
1.0 moles
GAS_PHASE 2
-fixed_pressure
-pressure 150.0
-temperature 50.0
CH4(g) 0.0
CO2(g) 0.0
H2(g) 0.0
SAVE solution 3
END

# ACF establish calcite saturation by the reaction
with sufficient amounts of calcite (saturation; SI
= 0) at at 40°C/100 atm
# before entering the carbonate reservoir rock
# OMP = 1.0 mol

USE solution 3
REACTION_PRESSURE 3
150
EQUILIBRIUM_PHASES 3
Calcite 0.0 100
Quartz 0.0 0.0 # potential newly formed mineral
Kaolinite 0.0 0.0 # potential newly formed mineral
GAS_PHASE 3
-fixed_pressure
-pressure 150.0
-temperature 50.0
CH4(g) 0.0
CO2(g) 0.0
H2(g)    0.0
END
```

STEP 2 SCENARIO 1.0 MOLES OMP – 50DEGCELSIUS – 150 BAR

```
#------------ 1.0 molal NaCl solution
SOLUTION 1
-pH 7.0
-temp 50.0
-units mol/kgw
Cl 1.000e+000
Na 1.000e+000

EQUILIBRIUM_PHASES 1
Calcite 0.0 100

REACTION_PRESSURE 1
150
END
```

STEP 3 SCENARIO 1.0 MOLES OMP – 50DEGCELSIUS – 150 BAR

```
# ACF (SI calcite = 0 at 150bar/50°C) enter the
carbonate reservoir
```

```
# 1D advective transport through the reservoir at
decreasing pressure/temperature

#---------------------- definition of additional
Acetate species from minteq.v4.dat
SOLUTION_MASTER_SPECIES
Acetate Acetate- 1.0 59.045 59.045

SOLUTION_SPECIES
Acetate- = Acetate-
 log_k 0

H+ + Acetate- = H(Acetate)
 log_k 4.757
 delta_h 0.41 kJ
 -gamma 0 0
 #         Id: 3309921
 #     log K source: NIST46.4
 #    Delta H source: NIST46.4
 #T and ionic strength: 0.00 25.0

Ca+2 + Acetate- = Ca(Acetate)+
 log_k 1.18
 delta_h 4 kJ
 -gamma 0 0
 #         Id: 1509920
 #     log K source: NIST46.4
 #    Delta H source: NIST46.4
 #T and ionic strength: 0.00 25.0

Na+ + Acetate- = Na(Acetate)
 log_k -0.18
 delta_h 12 kJ
 -gamma 0 0
 #         Id: 5009920
 #     log K source: NIST46.4
 #    Delta H source: NIST46.4
 #T and ionic strength: 0.00 25.0


K+ + Acetate- = K(Acetate)
 log_k -0.1955
 delta_h 4.184 kJ
 -gamma 0 0
 #         Id: 4109921
 #     log K source: NIST46.4
 #    Delta H source: NIST46.2
 #T and ionic strength: 0.10 25.0

#to print the calculated amounts of calcite in
different cells in an excel-file
Selected_Output
-file Scenario11.xls
-equilibrium_phases Calcite

#------------ Pore water prior to ACF infux (in
equilibrium with calcite)
SOLUTION 1
-pH 9.242
-pe -3.667
-temp 50
-units mol/kgw
C         9.561e-004
Ca        9.561e-004
Cl        1.000e+000
Na        1.000e+000

EQUILIBRIUM_PHASES 1
Calcite 0.0 100
Quartz 0.0 0 # potentially newly formed mineral
Kaolinite 0.0 0 # potentially newly formed mineral

REACTION_PRESSURE 1
150
REACTION_Temperature 1
50

GAS_PHASE 1
-fixed_pressure
-pressure 150.0
-temperature 50.0
CH4(g) 0.0
CO2(g) 0.0
H2(g) 0.0


SOLUTION 0 #Influx of ACF (SICalcite= 0) generated
at 85°C/305 bar from 1.0 mole OMP
-pH 4.127
-pe -1.433
-temp 50.0
-units mol/kgw
Acetate      9.572e-002
Al        1.886e-005
C        2.671e-001
Ca        2.697e-001
Cl        9.572e-001
K        1.237e-002
Na        4.630e-001
Si        1.693e-004

ADVECTION
-cells 1
-shifts 1000
END
```

GEOFLUIDS

Volume 16, Number 5, December 2016

ISSN 1468-8115

CONTENTS

WILEY Blackwell

Geofluids* is abstracted/indexed in *Chemical Abstracts

This journal is available online at Wiley Online Library.
Visit onlinelibrary.wiley.com to search the articles and register for table of contents and e-mail alerts.